

OPEN

Coherent response of the Indian Monsoon Rainfall to Atlantic Multi-decadal Variability over the last 2000 years

Pothuri Divakar Naidu^{1*}, Raja Ganeshram², Massimo A. Bollasina², Champoungam Panmei^{1,3}, Dirk Nürnberg⁴ & Jonathan F. Donges^{5,6}

Indian Summer Monsoon (ISM) rainfall has a direct effect on the livelihoods of two billion people in the Indian-subcontinent. Yet, our understanding of the drivers of multi-decadal variability of the ISM is far from being complete. In this context, large-scale forcing of ISM rainfall variability with multi-decadal resolution over the last two millennia is investigated using new records of sea surface salinity ($\delta^{18}\text{O}_w$) and sea surface temperatures (SSTs) from the Bay of Bengal (BoB). Higher $\delta^{18}\text{O}_w$ values during the Dark Age Cold Period (1550 to 1250 years BP) and the Little Ice Age (700 to 200 years BP) are suggestive of reduced ISM rainfall, whereas lower $\delta^{18}\text{O}_w$ values during the Medieval Warm Period (1200 to 800 years BP) and the major portion of the Roman Warm Period (1950 to 1550 years BP) indicate a wetter ISM. This variability in ISM rainfall appears to be modulated by the Atlantic Multi-decadal Oscillation (AMO) via changes in large-scale thermal contrast between the Asian land mass and the Indian Ocean, a relationship that is also identifiable in the observational data of the last century. Therefore, we suggest that inter-hemispheric scale interactions between such extra tropical forcing mechanisms and global warming are likely to be influential in determining future trends in ISM rainfall.

The Indian summer monsoon (ISM) is a large-scale coupled land-ocean-atmosphere phenomenon that plays a dominant role in transporting water vapour to the Indian subcontinent¹. Despite the strong bearing and societal relevance of the monsoon, reliable projections of ISM rainfall remain a challenge², mainly because of the complex dynamics and the myriad of interactions with other tropical and extra-tropical processes across various timescales³.

On a year to year basis, the ISM exhibits considerable complex and time-varying interactions with the El Niño/Southern Oscillation (ENSO)⁴, the Indian Ocean Dipole⁵ and Tibetan snow cover⁶. Additionally, intra-seasonal active or break events on short timescales, presumably associated with internal dynamics of the monsoon system itself, have large impacts on the interannual variability of monsoon rainfall^{7,8}. Example includes the famous break of July 2002, where rainfall was reduced by 50%⁹. These large year-to-year variations in rainfall associated with internal and external interactions pose a considerable challenge for Indian monsoon forecasting¹⁰ and for attributing monsoon variability to large-scale forcings. This is particularly true for multi-decadal and longer time scales given that observational data only covers few cycles and paleoclimate records span longer time scales which fill this gap.

There is currently a considerable debate on the impact of different forcing agents versus the role of internal variability in determining past and future long-term trends of the ISM¹¹. Global climate model experiments tend to suggest an intensification of the ISM in response to global warming partly because of the larger water-holding capacity of a warmer atmosphere, resulting in an estimated 10% increase by the end of the 21st century¹²; yet, there are large inter-model discrepancies (e.g., ref. ¹⁰). This is in striking contrast with the recent observational record, which indicates an overall decrease of the ISM rainfall during the period 1950–2012^{13–15}, followed by

¹CSIR-National Institute of Oceanography, Dona Paula, 403004, Goa, India. ²School of Geosciences, University of Edinburgh, Edinburgh, UK. ³Academy of Scientific and Innovative Research (AcSIR), CSIR-NIO, Goa, India. ⁴GEOMAR, Wischhofstrasse 1-3, 24148, Kiel, Germany. ⁵Postdam Institute for Climate Impact Research, P.O. Box 601203, D-14412, Postdam, Germany. ⁶Planetary Boundary Research Lab, Stockholm Resilience Center, Stockholm University, Stockholm, Sweden. *email: divakar@nio.org

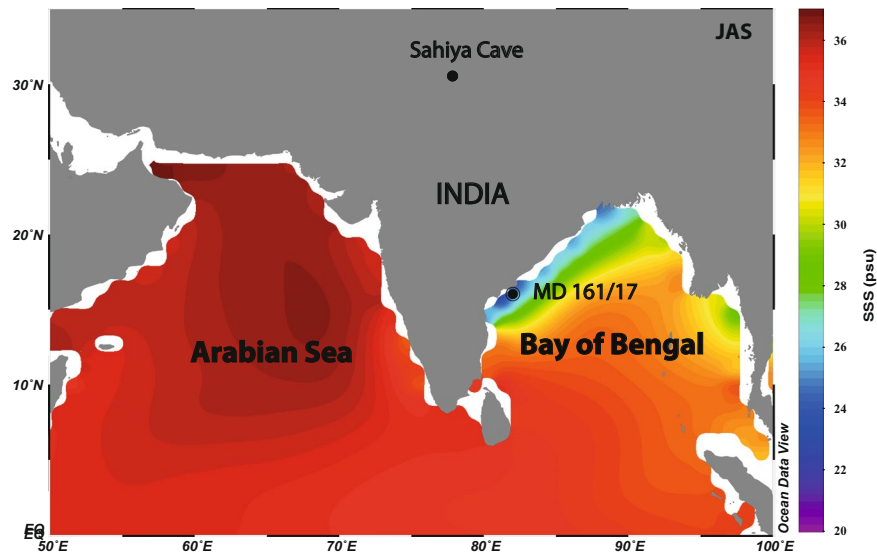


Figure 1. Location of MD161/17 Core and July through September salinity pattern in the northern Indian Ocean. Note MD161/17 Core was retrieved from the Krishna-Godavari Basin where a distinct low salinity prevails due the heavy over head precipitation and river discharge of Krishna, Godavari Rivers during Indian summer monsoon.

a weak revival between 2012–2014¹⁶. Decadal-scale internal climate variability associated with ENSO and the Atlantic Multi-decadal Oscillation (AMO) can also play an important role in explaining the observed variations in NH monsoon precipitation during the last century¹⁷ and possibly beyond^{18,19}. Thus a number of drivers, can contribute to modulating ISM rainfall, including internal variability of the climate system as well as interactions with natural and anthropogenic factors, either of global (e.g., greenhouse gases) or regional (e.g., anthropogenic aerosols and land-use) nature^{11,20–22}.

More integrated studies of the wider Northern Hemisphere (NH) summer monsoon suggest coherent changes of monsoon precipitation and circulation at hemispheric scales²³. The relatively coherent response of the various monsoons organised into the NH monsoon system to natural and anthropogenic forcing suggests that monsoon rainfall is sensitive to common hemispheric and/or planetary scale controls. Implicit in this view is the hypothesis that large-scale forcings may override regional-scale factors both natural and anthropogenic in determining future NH monsoon rainfall trends^{23,24}. Conversely, several studies also suggest a varying response of the individual monsoon systems to the same forcing due to internal feedback dynamics²⁵. Therefore, a better understanding of the large-scale controls of past decadal-scale variability of the monsoon is key to achieve more robust projections of its future changes. However, observations are spatially and temporally limited, mostly to the 20th century, which only allow identifying few long-term fluctuations¹⁷. Further extending these records back in time using paleoclimate reconstructions is essential to reduce current uncertainties, to identify its local and global scale forcing mechanisms, and to quantify the background monsoon variability on top of which shorter timescale fluctuations as well as longer-term anthropogenic-induced changes are superimposed²⁴. Here we present a new record of ISM rainfall and SST variability from the Northern Indian Ocean spanning the last 2,000 years at multi-decadal resolution and investigate the large-scale forcing mechanisms of ISM rainfall.

Salinity Variations in the Bay of Bengal

The Bay of Bengal (hereafter BoB; see Fig. 1) is a natural laboratory for reconstructing past ISM rainfall variations for two main reasons: Firstly, the BoB receives an estimated annual freshwater discharge of 2950 km³ from major (Ganges-Brahmaputra and Irrawaddy) and minor (Mahanadi, Krishna and Godavari) rivers fed by the ISM monsoon precipitation and glacier melt water²⁵. Thus the catchment of these rivers cover a large swath of the summer monsoon rainfall regions of North, Northeast and Central India. Secondly, the BoB directly receives heavy precipitation particularly in the northern parts. Precipitation plus runoff exceeds evaporation on an annual cycle. Fresh water from these sources is mixed into the upper layers of the BoB interacting with the surface circulation. After the summer monsoon some of the strongest lowering of seasonal salinity occurs along the Coromandel Coast in the northern and western BoB (Fig. 1). We exploited this prominent low salinity cap to reconstruct ISM rainfall and SST records from the Sediment Core MD161/17. The core site receives sediments from Mahanadi, Krishna and Godavari, and its tributaries, draining the northern portion of the Indian plateau, leading to enhanced sedimentation and expanded sediment sequence in the Krishna-Godavari Basin^{26,27}.

Proxy Records of Indian Monsoon Rainfall

In this study, we use Mg/Ca (SST) and $\delta^{18}\text{O}$ calcite ($\delta^{18}\text{O}_{\text{c}}$) from the calcite shells of planktonic foraminifera *Globigerinoides ruber* (hereafter *G. ruber*) to derive $\delta^{18}\text{O}_{\text{water}}$ ($\delta^{18}\text{O}_{\text{w}}$) to reconstruct ISM rainfall variability in the BoB at multi-decadal to centennial time scales (see suppl. material for further details). $\delta^{18}\text{O}_{\text{w}}$ exploits the higher $\text{O}^{16}/\text{O}^{18}$ isotopic ratios of precipitation associated with rainfall as opposed to sea water which has lower

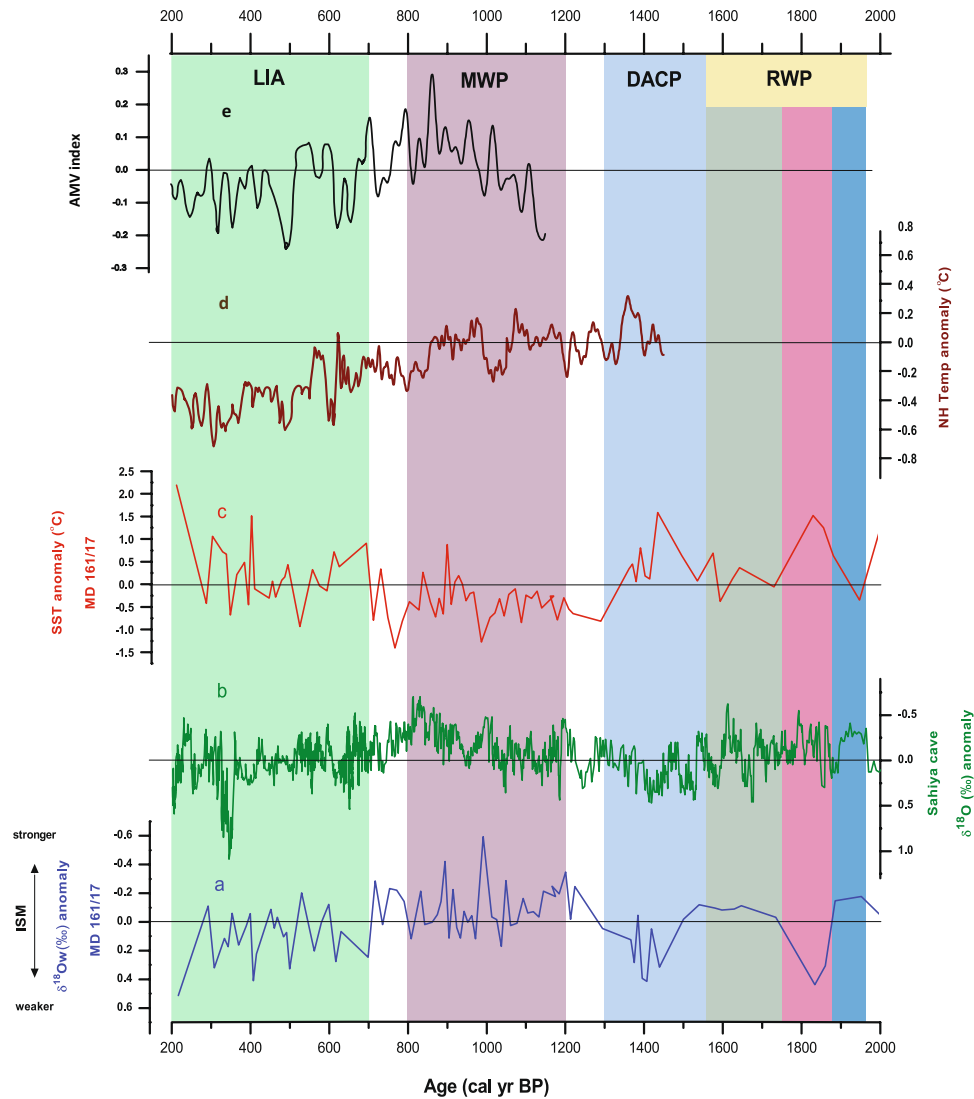


Figure 2. Variability of Indian summer monsoon rainfall over last two millennia; (a) $\delta^{18}\text{O}_w$ anomaly derived from $\delta^{18}\text{O}_c$ of Globigerinoides ruber from MD161/17 Core; (b) $\delta^{18}\text{O}_w$ anomaly of Sahiya Cave obtained from the $\delta^{18}\text{O}$ of speleothem¹⁹; (c) sea surface temperature anomaly from MD161/17 core obtained from the Mg/Ca ratios in Globigerinoides ruber; (d) Northern Hemisphere Air Temperature anomaly³², (e) Multi-decadal variability of Atlantic multi-decadal oscillations⁵¹.

$\text{O}^{16}/\text{O}^{18}$ ratios after appropriate corrections. On land, $\delta^{18}\text{O}$ of precipitation exhibits spatial variability and shows a negative relationship with precipitation which could vary over the monsoon season²⁴. However, the effects of such spatial and temporal variability are minimised in our study as the BoB receives rainfall from a large area of the Indian monsoon fed region and salinity anomalies persist over the monsoon and post monsoon periods. Also, the $\delta^{18}\text{O}_w$ and salinity show a strong positive relationship ($r^2 = 0.89$ with a slope of 0.15) in the BoB²⁸. Therefore, $\delta^{18}\text{O}_w$, at least in a qualitative sense, reflects salinity variations related to monsoon rainfall at the core site. Calcite tests of *G. ruber* are used for reconstructions because *G. ruber* fluxes from sediment trap time series from the BoB suggest that they record average surface conditions in the BoB²⁹. Previous studies have successfully used *G. ruber* to reconstruct ISM rainfall variability at millennial scale in the BoB since the last glacial period^{30,31}. High sedimentation rates (0.2 to 0.6 cm yr^{-1}) in Core MD161/17 allow us to reconstruct ISM rainfall variability at multi-decadal temporal resolution for the first time with robust chronology derived from 11 radiocarbon dates of mixed planktonic foraminifera species (Fig. S1).

Results

The $\delta^{18}\text{O}_w$ record shows a large variability (1.1‰) over the last 2000 years, with high and low $\delta^{18}\text{O}_w$ values representing decrease and increase of ISM rainfall respectively (Fig. S2). Figure 2a presents $\delta^{18}\text{O}_w$ as positive and negative anomalies over the mean of the record. Major portions of the Roman Warm Period (1950 to 1550 years before present (BP)); RWP) are associated with negative $\delta^{18}\text{O}_w$ anomalies, suggesting higher ISM rainfall. During Dark Age Cold Period (DACP) (1550 to 1300 year BP), high positive $\delta^{18}\text{O}_w$ anomalies are indicative of weaker

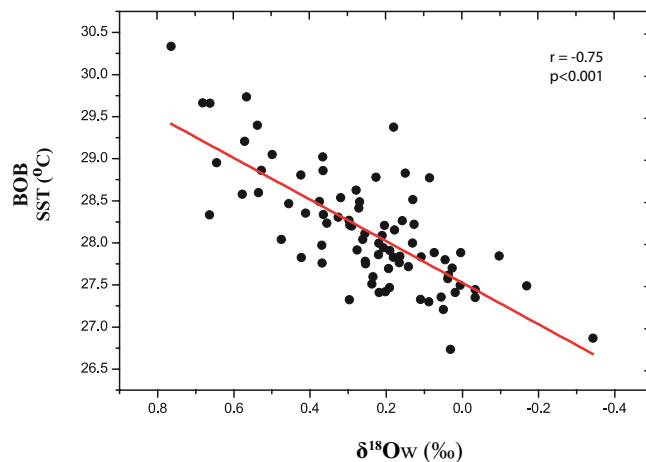


Figure 3. Relationship between the sea surface temperature and Indian Summer Monsoon Rainfall variability over last two millennia. Here the depleted and enriched $\delta^{18}\text{O}_w$ represent more and less ISM variability respectively. Note the significant negative correlation between the SST and ISM.

ISM rainfall. The Medieval Warm Period (MWP) from 1200 to 800 years BP is characterized by negative $\delta^{18}\text{O}_w$ anomalies compared to the preceding period (i.e. 2000 to 1300 years BP), which reveals that BoB experienced highest ISM rainfall and strong freshening during this MWP over the last 2000 years. In contrast, during the Little Ice Age (LIA), positive $\delta^{18}\text{O}_w$ anomalies indicate a decrease in ISM rainfall from 700 to 200 years BP. Our ISM rainfall record from the BoB shows similarity with the speleothem record from the Sahiya Cave (Fig. 2b) with statistically significant positive correlation at zero-lag (Fig. S3) reflecting continental rainfall over the Northern Himalayan foothills¹⁹ (Fig. 1). This confirms that our reconstructed variability in ISM rainfall is broadly representative of a large swath of Northern & Central India including the Indo-Gangetic plains.

Reconstructed SST from foraminiferal Mg/Ca ratios over the last 2000 years varies between 26.7° – 30.3°C (Fig. S2). SST anomalies are more than 1°C warmer during LIA and DACP and about 1°C cooler during the MWP as compared to the mean SST (Fig. 2c). Figure 3 shows the strong negative correlation between reconstructed ISM rainfall (represented by $\delta^{18}\text{O}_w$) and Mg/Ca based SST ($r = -0.75$; $p < 0.001$; $n = 84$). Cross correlation analyses of these two time series records also showed a significant negative correlation with zero-lag suggesting a strong temporal coupling between BoB SST and ISM rainfall over the last 2000 years at this core location (Fig. S4 and Table S2). In Fig. 2d, we compare the anomalies of ISM rainfall and BoB SST with the Northern Hemisphere surface air temperature (NHT) anomaly data of Mann and Jones³² for the last 1500 years. The composite NHT is derived from Atlantic and European regions but also include data from central and eastern Eurasian regions³⁰. Increased ISM rainfall and cooler BoB SSTs occur during periods of warmer NHT and vice versa (Fig. 2d). Also increased and decreased ISM rainfall during MWP and LIA corresponds with increase and decrease of AMO respectively (Fig. 2e). Kernel cross-correlation (red line) analysis of $\delta^{18}\text{O}_w$ anomaly (proxy of ISM rainfall) and NHT show significant positive correlation at zero year lag (Fig. S5). In summary, our reconstruction reveals the positive temporal relationship between ISM rainfall and Eurasian temperature, as well as the inverse relationship between ISM rainfall and BoB SST. In the following sections, we further explore these links by using recent (last 100 years) observations which, despite being temporally limited, provides extensive spatial coverage useful to understand the nature and mechanisms underpinning decadal ISM rainfall variability in our reconstructions of the last 2000 years.

Discussion

The Indian summer monsoon is a fully coupled ocean–land–atmosphere phenomenon whose fundamental driving mechanism can be identified in the differential heating between the land and the ocean to the south. During boreal spring, the land region over Asia and SE Asia warms faster than the ocean due to the lower heat capacity, setting up a low sea level pressure anomaly over Northern India and the Middle East. The resulting southward pressure gradient drives a cross-equatorial flow at the surface and a return flow aloft, forming a thermally-direct meridional cell⁸. A number of studies has found the Himalayas and Tibetan Plateau to also play an important thermal and mechanical role contributing to anchoring and intensifying the monsoon circulation by, respectively, heating the mid troposphere as well as by preventing cold air of mid-latitude origin to be advected to the south^{33,34}. The large-scale inter-hemispheric thermal contrast that develops in late-spring and early summer leads to the northward seasonal migration of the Inter-Tropical Convergence Zone¹⁰. A large proportion of monsoon rainfall falls over northeastern peninsular India and in other orographic hotspots such as the Western Ghats and Arakan Range of Myanmar³⁵. Once the monsoon is established over the Indian subcontinent, increased (land and ocean) evaporation and cloud cover lead to summertime cooling of the Indian Peninsula as well as of the north-equatorial Indian Ocean, with additional contribution from increased upwelling driven by the intense monsoon winds over its western sector¹. As the Himalayas acts as a physical barrier for the southerly moisture-laden flow, precipitation and associated surface cooling are confined largely to the Indian Subcontinent, while the Tibetan Plateau is mainly dry and warm³⁵. This maintains the meridional temperature

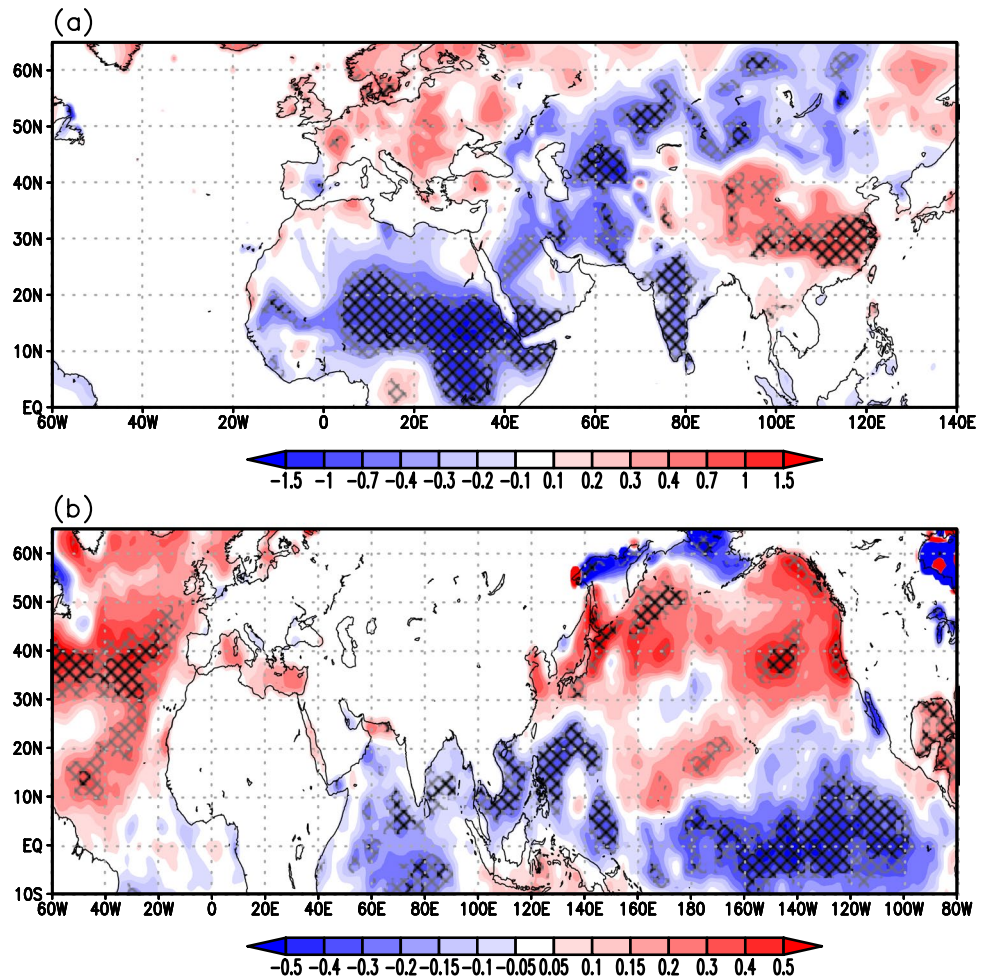


Figure 4. Regressions of observed low-pass filtered June-September (JJAS) mean (a) surface temperature ($^{\circ}\text{C}$) and (b) sea-surface temperature ($^{\circ}\text{C}$) on observed JJAS All-India summer monsoon rainfall during 1901-2012. All data were linearly detrended prior to the analysis. The analysis focuses on decadal or longer scale variability, isolated by applying a low-pass Lanczos filter with a cut-off frequency of 10 years to JJAS-mean data. The cross-hatching marks regions where the correlation exceeds the 90% (grey) and 95% (black) confidence levels, estimated by using a Monte Carlo approach with 1,000 random samples of the time series⁶⁸. Land temperature data are from the Climate Research Unit (CRU), University of East Anglia, United Kingdom, dataset (CRU-TS3.21) at $0.5^{\circ} \times 0.5^{\circ}$ resolution⁶⁹, while sea surface temperature are from the Hadley Centre Sea Ice and Sea Surface Temperature data set (HadISST) dataset version 1 at $0.5^{\circ} \times 0.5^{\circ}$ resolution⁷⁰. Rainfall data are taken from the homogeneous rainfall data set of 306 raingauges in India, developed by the Indian Institute of Tropical Meteorology⁷¹.

gradient sustaining monsoon circulation and rainfall during the summer monsoon season³⁶. Our reconstructions shown in Fig. 2a,c capture two key characteristics of the fundamental mechanics underpinning the annual cycle of the ISM¹: salinity variations in the BoB reflecting monsoon rainfall and freshwater flux and² lowering of the surface SSTs of the northern Indian Ocean during the monsoon period representing evaporative cooling associated with intensified monsoon winds and cloud cover. The inverse relationship (Fig. 3) and the coherent response (Fig. 2a,c) of these two reconstructed elements provide assurance that the changes we see are related to ISM variability. Furthermore, the close correspondence between these reconstructions and the NHT records (Fig. 2d,e) support the causal link between NH temperature and ISM rainfall via seasonal changes in the meridional surface/tropospheric thermal gradients^{23,24}.

Drivers of Multi-decadal ISM Rainfall Variability

We further explore the link between large-scale temperature changes and ISM variability at multi-decadal scale by means of observational data during 1901–2012. To make a direct comparison with the multi-decadal proxy records we remove interannual and short time scale variability in the observational data by low-pass filtering. This isolates the decadal or longer time-scale components of the signal from higher-frequency variability which is known to be largely influenced by internal monsoon dynamics¹⁰. The purpose of using observational data here is twofold¹: to evaluate whether seasonal features such as cooling of the BoB related to monsoon circulation are represented in decadal time scales and² to identify large-scale forcing mechanisms of All-India Monsoon Rainfall

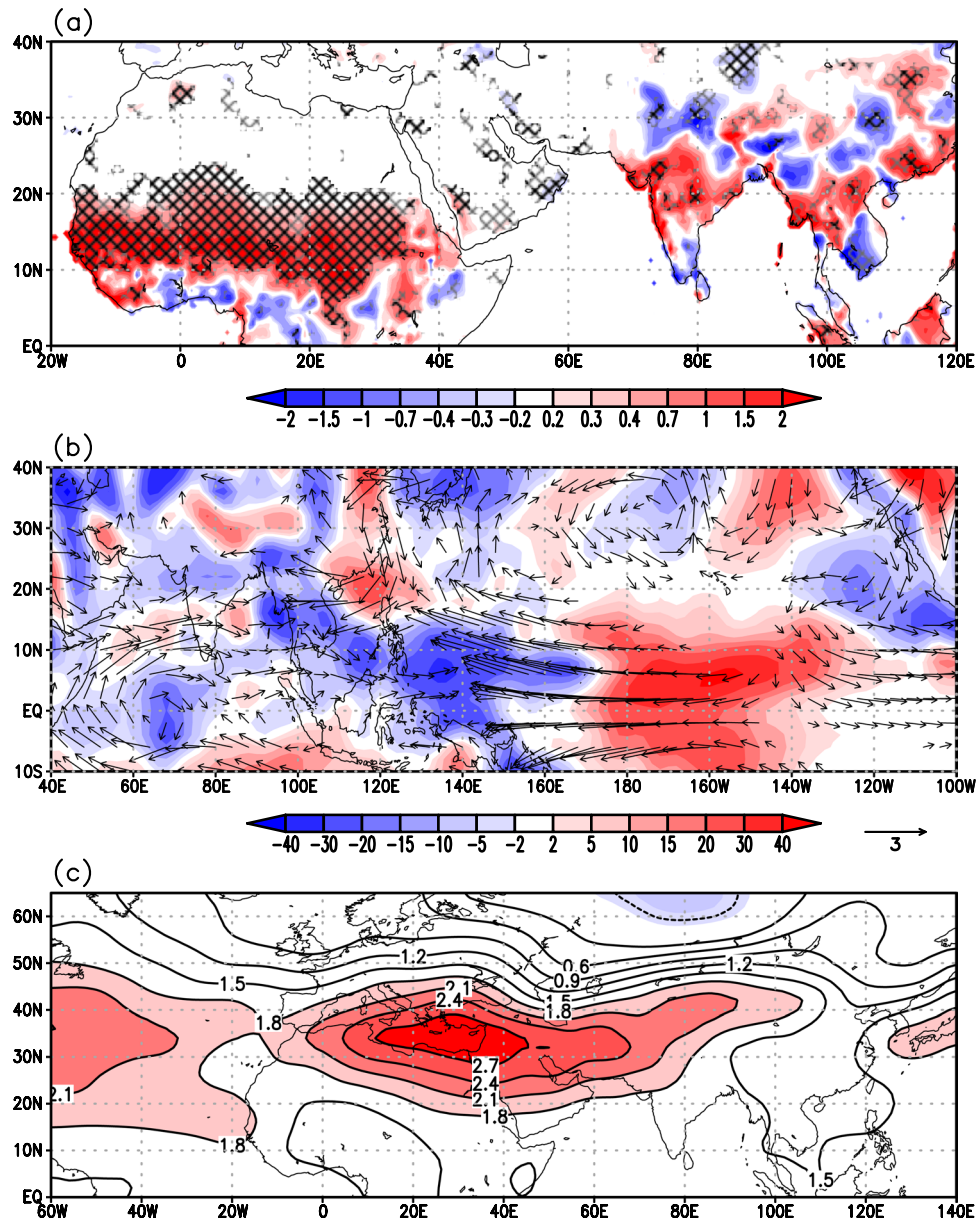


Figure 5. Regressions of observed low-pass filtered June-September (JJAS) mean (a) precipitation (mm day⁻¹), (b) 500-hPa vertical velocity (hPa day⁻¹) and 850-hPa winds (m s⁻¹), where blue and red areas represent ascending and descending air masses respectively, (c) mean upper-tropospheric (200 – 500 hPa) air temperature (°C) on the AMO index shown in Fig. 6 during 1901–2012. All data were linearly detrended prior to the analysis. Precipitation data are from the CRU-TS3.21 dataset, while winds and air temperature are from NOAA-CIRES 20th Century Reanalysis dataset. Anomalies are given per °C change of the AMO. The cross-hatching marks regions where the correlation exceeds the 90% (grey) and 95% (black) confidence levels, estimated by using a Monte Carlo approach with 1,000 random samples of the time series.

(AIMR) fluctuations at these time scales. Figure 4 presents the spatial map of June-September (JJAS) surface temperature anomalies associated with decadal or longer variations in the AIMR. At the surface, excess AIMR is associated with significant positive temperature anomalies over Eurasia and in particular eastern Asia and the Tibetan Plateau (Fig. 4a) and negative temperature anomalies over the Indian Subcontinent and the Tropical Indian Ocean (Fig. 4b). The elevated heating over the Tibetan Plateau, concurrently with slight cooling of the north equatorial Indian Ocean, has been identified as a dominant factor driving the annual cycle and interannual variability of the monsoon system^{7,37}. Further afield, a strong positive association between ISM rainfall and SST anomalies in the North Atlantic Ocean and surface temperature over western Eurasia is evident in Fig. 4b³⁸. Large basin-wide sea surface temperature anomalies are also identifiable across the Pacific, with cooling along the equatorial central-eastern Pacific, and an extensive warming in the extra tropics stretching from Japan to the western coast of the US. The tropical anomalies are somewhat reminiscent of a La Niña-like cooling in the eastern equatorial Pacific. However, the pattern also features substantial differences in two important and fundamental

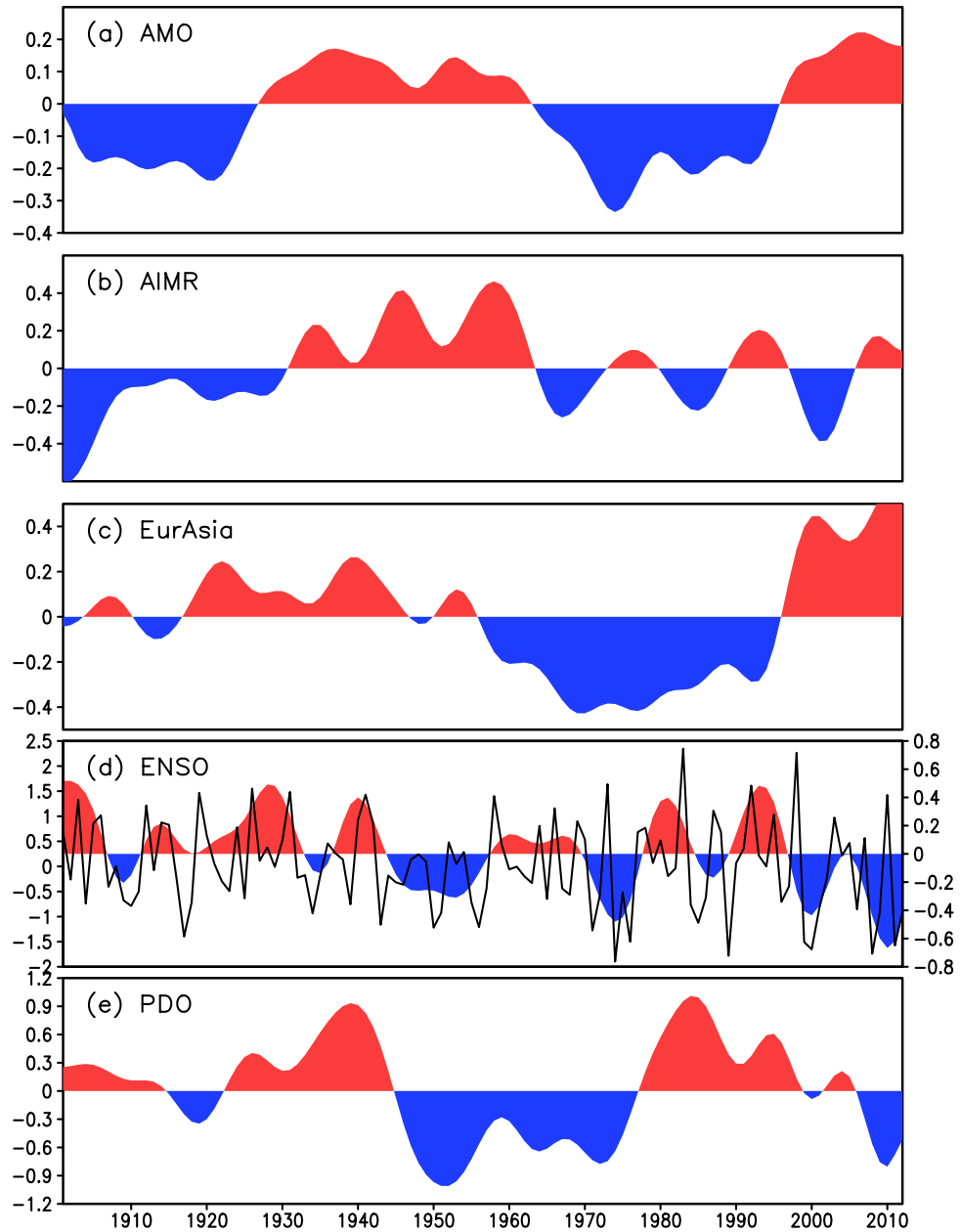


Figure 6. Time series of observed low-pass filtered (a) Atlantic Multidecadal Oscillation (AMO) index ($^{\circ}\text{C}$), (b) June–September (JJAS) All-India summer monsoon rainfall anomalies (mm day^{-1}), (c) JJAS surface temperature anomalies ($^{\circ}\text{C}$) over Eurasia (20° – 140°E , 30° – 75°N), (d) December–February Niño3.4 index ($^{\circ}\text{C}$, right y-axis), and (e) standardised annual mean Pacific Decadal Oscillation index during 1901–2012. All data were linearly detrended prior to the analysis. The analysis focuses on decadal or longer scale variability, isolated by applying a low-pass Lanczos filter with a cut-off frequency of 10 years to the detrended data. Land temperature data are from the Climate Research Unit (CRU), University of East Anglia, United Kingdom, dataset (CRU-TS3.21) at $0.5^{\circ} \times 0.5^{\circ}$ resolution⁶⁸, while sea surface temperature are from the Hadley Centre Sea Ice and Sea Surface Temperature data set (HadISST) dataset version 1 at $0.5^{\circ} \times 0.5^{\circ}$ resolution⁶⁹. Rainfall data are taken from the homogeneous rainfall data set of 306 rain gauges in India, developed by the Indian Institute of Tropical Meteorology⁷⁰. The AMO index is defined as the area average over the North Atlantic (80°W – 0°E , 0° – 60°N) of annual mean sea surface temperatures¹⁷. The Niño3.4 index is calculated by averaging the time series of sea surface temperature (SST) anomalies over (5°S – 5°N , 170° – 120°W), with SST coming from the HadISST dataset as in Fig. 4. The unfiltered (yearly) values of the Niño3.4 index are also plotted in (a) as the continuous black line (left y-axis). The PDO index (obtained from <http://research.jisao.washington.edu/pdo/PDO.latest>) is derived as the leading principal component of monthly sea surface temperature anomalies in the North Pacific Ocean, poleward of 20°N . The monthly mean global average SST anomalies are removed to separate this pattern of variability from any global warming signal that may be present in the data.

characteristics of the actual La Niña sea surface temperatures anomalies or of its longer-lived manifestation, the Pacific Decadal Oscillation (PDO)³⁹. First, it does not display zonal opposite-sign SST anomalies over the western equatorial Pacific, and second, the anomalies do not extend over the northeastern Pacific. We will return to this point later. Overall, this corroborates the assembled paleo-reconstructions presented in Fig. 2 and allows us to place ISM rainfall variability over the last 2000 years in the wider context of mechanisms associated with NH climate variability.

The AMO has been suggested to have played a major role in modulating hemispheric-scale temperature gradients at multi-decadal time scales during the last 2000 years^{40,41} via its link with Atlantic Thermohaline Circulation (THC) variations and associated inter-hemispheric heat transport fluctuations^{42,43}. The AMO has also been suggested to play a major role in modulating the 20th century multi-decadal variations of Indian and African (Sahel) summer rainfall, as well as the tropical Atlantic atmospheric circulation (e.g., refs. 17,44). Figure 5 shows regression/correlation patterns of JJAS precipitation (Fig. 5a), three-dimensional circulation (Fig. 5b), and upper-tropospheric temperature anomalies (Fig. 5c) on the AMO. A positive AMO phase is associated with overall increased precipitation over the Indian subcontinent, with a large positive anomaly over central India (peak values statistically significant at the 95% level) and reduced precipitation to the south and over the central Himalayas (Fig. 5a). This pattern is associated with stronger low-tropospheric southwesterly winds over the Arabian Sea bringing more moisture toward India (Fig. 5b). The mid- and upper-tropospheric heating anomaly (Fig. 5c) features significant warming from the Atlantic across northern Africa to the Middle East and northern India, which intensifies the meridional thermal contrast between the continent and the Indian Ocean—a pattern consistent with several other modelling studies^{45,46}. The regional circulation anomalies associated with the southwesterlies in the northern Indian Ocean are part of a hemispheric-wide response pattern to AMO variability featuring enhanced easterly trade winds across the northern equatorial Pacific and enhanced Walker cell north of the equator, leading to larger ascent (precipitation) over Indo-China and the Maritime Continent and subsequent changes in the meridional direction (regional Hadley circulation). These patterns, including the Indo-Pacific sea surface temperature anomalies, bear remarkable similarity to those described in previous studies⁴⁷ and related to variations in the Atlantic oceanic circulation. Figure 5b also displays an interesting wave pattern in the ascending and descending air masses in the northern hemisphere extratropics which some have indicated as responsible for the propagation of the AMO signal from the Atlantic across Eurasia (e.g., ref. 48). This analysis, albeit not exhaustive, is suggestive of an AMO-ISM teleconnection with signatures of both an atmospheric pathway via modulation of the upper-tropospheric temperature across Eurasia (e.g. 45,48–50), and one that also involves atmosphere-ocean feedbacks in the Indo-Pacific region (e.g. 47,51). Overall, this is indicative of an AMO imprint on the global interhemispheric temperature gradient with a positive phase of the AMO associated with a warmer NH than the SH (Fig. 4b), with ensuing modulation of the NH monsoon systems. We explore this further using palaeoclimate and observational time series.

The time series displayed in Fig. 6a–c show that, in general, decadal-scale wet periods over India (e.g., 1926–1965) are in phase with a positive AMO (warmer North Atlantic SSTs) and warmer Asian surface temperature anomalies; conversely, dry periods of the ISM (i.e., 1901–1926 and 1965–1995) occur simultaneously with a negative phase of the AMO and cooler Asian surface temperature anomalies. Such forcing mechanism and distal teleconnections appear to be at play also during the last 2000 years based on our paleo-monsoon reconstructions (Fig. 2) revealing a coherent response between AMO and ISM, further substantiating previous studies based on sparse monsoon records^{24,52}. On millennial to century time scales, ISM strength has been correlated with Dansgaard–Oeschger cycles in Greenland ice cores, where weak monsoon events are associated with cold events in the NH during the last glaciation and the Holocene^{52–56}. Such weakening of the ISM has been related to Northern hemispheric cooling resulting from ice-sheet instability inducing changes in the Atlantic THC^{32,57}. Therefore, a strong relationship between NHT and Indian monsoon variability appears to be a persistent and coherent feature of the past and observed climate at decadal or longer time scales.

In contrast, the association of ISM rainfall with ENSO/Pacific Decadal Oscillation (PDO) is poor in both observational data (Fig. 6d,e) and palaeoclimate records on multi-decadal time scales (Figs. S7 and S8). This is in contrast with one recent study of the last 500 years, which revealed that AMO, ISM rainfall and ENSO exhibit a common 50–80 year variability suggesting that this mode is an integral part of global multi-decadal oscillations arising from large scale coupled ocean-atmosphere-land interactions⁵⁸. Collectively, such discordance suggests that ENSO forcing on ISM rainfall is time varying and complex as suggested by several recent studies^{59,60}. This is perhaps because ENSO forcing mechanism operates mainly on higher frequencies on which internal dynamics of monsoon itself dominates and hence not always detected in longer time scales. High frequency variability in rainfall associated with the ENSO⁴, the Indian Ocean Dipole⁵ and Tibetan snow cover⁶ are relatively small, the interannual standard deviation of summer-mean rainfall being around 10% of the climatological mean¹⁰. Observational data also suggest that the decadal pattern of ocean-atmospheric oscillations of the Pacific Ocean do not conform with the typical ENSO or PDO modes (e.g., Figs. 4b and 5b). Further investigations are required to understand fully the nature of this oscillation pattern.

In summary, we suggest that multi-decadal ISM rainfall variability during the last 2000 years was modulated by AMO related fluctuations in NH temperatures whereby warmer (cooler) Asian landmasses along with a cooler (warmer) Indian Ocean set up stronger (weaker) surface and tropospheric meridional temperature gradients strengthening (weakening) monsoon circulation and rainfall. Therefore, the reconstructed temporal relationships between ISM rainfall, BoB SST and NHT over the last 2000 years allow to extend and strengthen the findings based on the rather limited observational record for the 20th century shedding light on distal teleconnections underpinning multi-decadal ISM variations. It is interesting to note that Fig. 6 suggests a weakening of the AMO-ISM relationship from the mid-1990s, when the AMO entered a positive phase while the ISM rainfall remained below average (ref. 17 Fig. 6). This recent decoupling is discussed further in the context of anthropogenic forcing.

Implications for ISM Variations Under Anthropogenic Forcing

Our results suggesting a link between the AMO and the associated NH differential warming and ISM rainfall variability at multi-decadal timescales during the last 2 millennia have important implications for the current debate on the future evolution of ISM rainfall in response to global warming. Our study strongly supports the notion that multi-decadal variations of ISMR are sensitive to extra tropical forcing that occurs beyond regional scales. It is also on these timescales that anthropogenic forcing can interact with internal variability of the monsoon. Broadly, AMO forcing on the monsoon acts by changing inter-hemispheric thermal gradients (Fig. 4). NH warming associated with positive phases of this oscillation enhances meridional pressure gradients that drive cross-equatorial flows and intensify NH monsoon circulation and rainfall¹⁷ (Fig. 5). Global warming trends since the early seventies have been asymmetric across the hemispheres, with the NH warming faster than the SH^{23,61}. The interaction between this global warming pattern and positive phases of the AMO would further accentuate the inter-hemispheric thermal contrast, reinforcing NH temperature positive anomalies and intensifying NH monsoon circulation and rainfall. The post mid-1990s decoupling of ISM from AMO (Fig. 6) has been widely attributed to the influence of aerosols and land use changes^{8,11,19}. In view of our results, such regional influences dampening ISMR are likely to be temporary depending partly on future levels of these aerosol emission and land use change. On longer time scales, NH temperature anomalies will have an overriding influence on enhancing monsoon. In this regard, we note that ISM rainfall registered a recovery since 2002 with above average rainfall after 2012^{2,23,43,62}. Finally, we suggest that interaction between AMO and global warming is likely to be a crucial factor in ISM rainfall trajectory into the future. Therefore, large-scale interactions involving extratropical factors in response greenhouse gas warming cannot be ignored in future ISM rainfall prediction.

Methods Summary

Core MD161/17 was collected at a water depth of 790 m from the KGB. Age model was based on linear interpolation between 11 AMS radiocarbon dates which cover a time span of 2 kyr (Supplementary Table 2). *Globigerinoides ruber* (150 to 250 μm) was analyzed for $\delta^{18}\text{O}$ by reacting with 100% orthophosphoric acid at a constant 75 °C in a Kiel Carbonate III preparation device and evolved CO_2 gas was analyzed by using Thermo Electron delta plus advantage stable isotope ratio mass spectrometer. Cleaning protocol of *G. ruber* for Mg/Ca analyses were followed by Barker *et al.*⁶³, in addition a reductive cleaning step was used according to Martin and Lea⁶⁴. Mg/Ca ratios were measured by using an axial viewing Varian 720 ICP-OES (for details see the supplementary material). Mg/Ca values were then used to estimate SSTs using the equation $\text{Mg/Ca} = 0.449\exp(0.09 \cdot \text{T})$ ⁶⁵. $\delta^{18}\text{O}_{\text{sw}}$ were computed by applying the following equation of Bemis *et al.*⁶⁶: $\delta^{18}\text{O}_{\text{sw}} = 0.27 \cdot (\text{T} - 16.5 + 4.8 \cdot \text{d}18\text{O}) / 4.8$. The derived $\delta^{18}\text{O}_{\text{sw}}$ estimates were corrected for continental ice volume using Shackleton's data set⁶⁷ and presented here as $\delta^{18}\text{O}_{\text{sw}}$. SST and $\delta^{18}\text{O}_{\text{sw}}$ anomalies are computed by subtracting the mean values of all data points within two millennia from the SST and $\delta^{18}\text{O}_{\text{sw}}$ values respectively.

Received: 6 February 2019; Accepted: 21 December 2019;

Published online: 28 January 2020

References

- Loschnigg, J. & Webster, P. J. A coupled ocean-atmosphere system of SST modulation for the Indian Ocean. *J. Clim.* **13**, 3342–3360 (2000).
- Asharaf, S. & Ahrens, B. Indian summer monsoon rainfall processes in climate change scenarios. *J. Clim.* **28**(13), 5414–5429 (2015).
- Zhisheng, A. *et al.* Global monsoon dynamics and climate change. *Annu. Rev. Earth. Planet. Sci.* **43**(1), 29–77 (2015).
- Pant, G. B. & Parthasarathy, S. B. Some aspects of an association between the southern oscillation and Indian summer monsoon. *Arch. Meteorol. Geophys. Bioclim., Series B*, **29**(3), 245–252 (1981).
- Abram, N. J. *et al.* Seasonal characteristics of the Indian Ocean Dipole during the Holocene epoch. *Nature* **445**, 299–302 (2007).
- Li, W. *et al.* Influence of Tibetan Plateau snow cover on East Asian atmospheric circulation at medium-range time scales. *Nat. Commun.* **9**, 4243 (2018).
- Webster, P. J. *et al.* Monsoons: Processes, predictability, and the prospects for prediction. *J. Geophys. Res. Oceans* **103**, 14451–14510 (1998).
- Gadgil, S. The Indian Monsoon and its variability. *Annu. Rev. Earth. Planet. Sci.* **31**(1), 429–467 (2003).
- Bhat, G. S. Indian drought of 2002 — a sub-seasonal phenomenon? *Q. J. R. Meteorol. Soc.* **132**, 2583–2602 (2006).
- Turner, A. G. & Annamalai, H. Climate change and the South Asian summer monsoon. *Nat. Clim. Change* **2**, 587–595 (2012).
- Roxy, M. K. *et al.* A threefold rise in widespread extreme rain events over central India. *Nat. Commun.* **8**, 708 (2017).
- Menon, A., Levermann, A., Schewe, J., Lehmann, J. & Frieler, K. Consistent increase in Indian monsoon rainfall and its variability across CMIP-5 models. *Earth Syst. Dynam.* **4**, 287–300 (2013).
- Guhathakurta, P. & Rajeevan, M. Trends in the rainfall pattern over India. *Int. J. Clim.* **28**(11), 1453–1469 (2008).
- Kitoh, A. *et al.* Monsoons in a changing world: A regional perspective in a global context. *J. Geophys. Res. Atmos.* **118**(8), 3053–3065 (2013).
- Zhou, T., Yu, R., Li, H. & Wang, B. Ocean forcing to changes in global monsoon precipitation over the recent half-century. *J. Clim.* **21**(15), 3833–3852 (2008).
- Jin, Q. & Wang, C. A revival of Indian summer monsoon rainfall since 2002. *Nat. Clim. Change* **7**, 587–594 (2017).
- Zhang, R. & Delworth, T. L. Impact of Atlantic multidecadal oscillations on India/Sahel rainfall and Atlantic hurricanes. *Geophys. Res. Lett.* **33**, L17712 (2006).
- Knudsen, M. F., Seidenkrantz, M.-S., Jacobsen, B. H. & Kuijpers, A. Tracking the Atlantic Multidecadal Oscillation through the last 8,000 years. *Nat. Commun.* **2**, 178 (2011).
- Kathayat, G. *et al.* The Indian monsoon variability and civilization changes in the Indian subcontinent. *Sci. Adv.* **3**(12), e1701296 (2017).
- Bollasina, M. A., Ming, Y. & Ramaswamy, V. Anthropogenic aerosols and the weakening of the South Asian summer monsoon. *Science* **28**, 502–505 (2011).
- Polson, D., Bollasina, M., Hegerl, G. C. & Wilcox, L. J. Decreased monsoon precipitation in the Northern Hemisphere due to anthropogenic aerosols. *Geophys. Res. Lett.* **41**, 6023–6029 (2014).
- Roxy, M. K. *et al.* Drying of Indian subcontinent by rapid Indian Ocean warming and a weakening land-sea thermal gradient. *Nat. Commun.* **6**, 7423 (2015).

23. Wang, B. *et al.* Northern hemisphere summer monsoon intensified by mega-El Niño/southern oscillation and Atlantic multidecadal oscillation. *Proc. Nat. Acad. Sci.* **110**, 5347–5352 (2013).
24. Sinha, A. *et al.* Trends and oscillations in the Indian summer monsoon rainfall over the last two millennia. *Nat. Comms.* **6**, 6309 (2015).
25. Sengupta, D., Bharath Raj, G. N. & Shenoi, S. S. C. Surface freshwater from Bay of Bengal runoff and Indonesian Throughflow in the tropical Indian Ocean. *Geophys. Res. Lett.* **33**(22), 1–5 (2006).
26. Forsberg, C. F., Solheim, A., Kvalstad, T. J., Vaidya, R. & Mohanty, S. Slope instability and mass transport deposits on the Godavari river delta, east Indian margin from regional geological perspective, Lykousis, V., Sakellariou, Locat, J., (Eds.) (2013).
27. Frierson, D. M. W. *et al.* Contribution of ocean overturning circulation to tropical rainfall peak in the Northern Hemisphere. *Nat. Geosci.* **6**(11), 940–944 (2007).
28. Sengupta, S., Parekh, A., Chakraborty, S., Ravi Kumar, K. & Bose, T. Vertical variation of oxygen isotope in Bay of Bengal and its relationships with water masses. *J. Geophys. Res.: Oceans* **118**, 6411–6424 (2013).
29. Guptha, M. V. S., Curry, W. B., Ittekkot, V. & Muralinath, A. S. Seasonal variation in the flux of Planktic foraminifera: sediment trap results from the Bay of Bengal, Northern Indian Ocean. *J. Foraminiferal Res.* **27**, 5–19 (1997).
30. Govil, P. & Naidu, P. D. Variations of Indian monsoon precipitation during the last 32kyr reflected in the surface hydrography of the Western Bay of Bengal. *Quat. Sci. Rev.* **30**(27–28), 3871–3879 (2011).
31. Rashid, H., Flower, B. P., Poore, R. Z. & Quinn, T. M. A ~25 ka Indian Ocean monsoon variability record from the Andaman Sea. *Quat. Sci. Rev.* **26**(19–21), 2586–2597 (2007).
32. Mann, M. E. & Jones, P. D. Global surface temperatures over the past two millennia. *Geophys. Res. Lett.* **30**(15), 15–18 (2003).
33. Goswami *et al.* The Annual Cycle, Intraseasonal Oscillations, and Roadblock to Seasonal Predictability of the Asian Summer Monsoon. *J. Clim. Special Section* **19**, 5078–5099 (2006).
34. Wu, G. *et al.* Thermal controls on the Asian summer monsoon. *Sci. Rep.* **2**(404), 1–7 (2012).
35. Choudhury, A. D. & Krishnan, R. Dynamical response of the South Asian monsoon trough to latent heating from stratiform and convective precipitation. *J. Atmos. Sci.* **68**, 1347–1363 (2011).
36. Xavier, P. K., Marzin, C. & Goswami, B. N. An objective definition of the Indian summer monsoon season and a new perspective on the ENSO-monsoon relationship. *Q. J. R. Meteorol. Soc.* **133**, 749–764 (2007).
37. Boos, W. R. & Kuang, Z. Dominant control of the South Asian monsoon by orographic insulation versus plateau heating. *Nature* **463**, 218–222 (2010).
38. Li, C. & Yanai, M. The onset and interannual variability of the Asian Summer Monsoon in relation to land-sea thermal contrast. *J. Clim.* **9**, 358–375 (1996).
39. Deser, C., Alexander, M. A., Xie, S. P. & Phillips, A. S. Sea surface temperature variability: Patterns and mechanisms. *Annu. Rev. Mar. Sci.* **2**, 115–143 (2010).
40. Delworth, T. L. & Mann, M. E. Observed and simulated multi-decadal variability in the Northern Hemisphere. *Clim. Dyn.* **16**, 661–676 (2000).
41. Mann, M. E. *et al.* Global signatures and dynamical origins of the Little Ice Age and Medieval climate anomaly. *Science* **326**, 1256–1259 (2009).
42. Clement, A. *et al.* The Atlantic Multidecadal Oscillation without a role for ocean circulation. *Science* **350**(6258), 320–324 (2015).
43. Zhang, X., Knorr, G., Lohmann, G. & Barker, S. Abrupt North Atlantic circulation changes in response to gradual CO₂ forcing in a glacial climate state. *Nat. Geosci.* **10**, 518–523 (2017).
44. Park, J.-Y., Bader, J. & Matei, D. Northern-hemispheric differential warming is the key to understanding the discrepancies in the projected Sahel rainfall. *Nat. Comms.* **6**, 5985 (2015).
45. Goswami, B. N., Madhusoodanan, M. S., Neema, C. P. & Sengupta, D. A physical mechanism for North Atlantic SST influence on the Indian summer monsoon. *Geophys. Res. Lett.* **33**(2), 1–4 (2006).
46. Luo, F. *et al.* The Connection between the Atlantic Multidecadal Oscillation and the Indian Summer Monsoon since the Industrial Revolution Is Intrinsic to the Climate System. *Environmental Research Letters* **13**(9), 094020, <https://doi.org/10.1088/1748-9326/aade11> (2018).
47. Zhang, R. & Delworth, T. L. Simulated tropical response to a substantial weakening of the Atlantic thermohaline circulation. *J. Climate* **18**, 1853–1860 (2005).
48. Luo, F., Li, S. & Fur evik, T. The connection between the Atlantic Multidecadal Oscillation and the Indian Summer Monsoon in Bergen Climate Model Version 2.0. *J. Geophys. Res.* **116**, D19117, <https://doi.org/10.1029/2011JD015848> (2011).
49. Krishnamurthy, L. & Krishnamurthy, V. Teleconnections of Indian monsoon rainfall with AMO and Atlantic tripole. *Clim. Dyn.* **46**, 2269–85 (2016).
50. Wang, Y., Li, S. & Luo, D. Seasonal response of Asian monsoonal climate to the Atlantic Multidecadal Oscillation. *J. Geophys. Res.* **114**, D02112, <https://doi.org/10.1029/2008JD010929> (2009).
51. Lu, R., Dong, B. & Ding, H. Impact of the Atlantic Multidecadal Oscillation on the Asian summer monsoon. *Geophys. Res. Lett.* **33**, L24701, <https://doi.org/10.1029/2006GL027655> (2006).
52. Knudsen, M. F., Seidenkrantz, M. A., Jacobsen, B. H. & Kuijpers, A. Tracking the Atlantic Multi-decadal oscillations through the last 8000 years. *Nat. Comms.* doi:10.1038 (2011).
53. Schulz, H., van Rad, U. & Erlenkeuser, H. Correlation between Arabian Sea and Greenland climate oscillations of the past 110,000 years. *Nature* **393**, 54–57 (1998).
54. Sinha, A. *et al.* Variability of Southwest Indian summer monsoon precipitation during the Bølling-Ållerød. *Geology* **33**(10), 813–816 (2005).
55. Ivanochko, T. S. *et al.* Variations in tropical convection as an amplifier of global climate change at millennial scale. *Earth. Planet. Sci. Lett.* **235**, 302–314 (2005).
56. Gupta, A. K., Das, M. & Anderson, D. M. Solar influence on the Indian summer monsoon during the Holocene. *Geophys. Res. Lett.* **32**, L17703 (2005).
57. Clement, A. C. & Peterson, L. C. Mechanisms of abrupt climate change of the last glacial period. *Rev. Geophys.* **46**, RG4002 (2008).
58. Goswami, B. N., Kripalani, R. H., Borgoankar, H. P. & Preethi, B. Multi-decadal variability in Indian summer monsoon rainfall using proxy data. *Climate Change: Multidecadal and Beyond*, Chang, C.-P. *et al.* Eds., World Scientific Series on Asia-Pacific Weather and Climate, Vol. 6, 327–345 (2015).
59. Yun, K.-S. & Timmermann, A. Decadal monsoon-ENSO relationships reexamined. *Geophys. Res. Lett.* **45**, 2014–2021 (2018).
60. Tejavath, C. T., Ashok, K., Chakraborty, S. & Ramesh, R. A PMIP3 narrative of modulation of ENSO teleconnections to the Indian summer monsoon by background changes in the last millennium. *Clim. Dyn.* <https://doi.org/10.1007/s00382-019-04718> (2019).
61. Robeson, S. M., Willmott, C. J. & Jones, P. D. Trends in hemispheric warm and cold anomalies. *Geophys. Res. Lett.* **41**, 9065–9071 (2014).
62. Wang, B. *et al.* Rethinking Indian monsoon rainfall prediction in the context of recent global warming. *Nat. Comms.* **6**, 7154 (2015).
63. Barker, S., Greaves, M. & Elderfield, H. A study of cleaning procedures used for foraminiferal Mg/Ca paleothermometry. *Geochem. Geophys. Geosyst.* **4**(9), 1–20 (2003).
64. Martin, P. A. & Lea, D. W. A simple evaluation of cleaning procedures on fossil benthic foraminiferal Mg/Ca. *Geochem. Geophys. Geosyst.* **3**(10), 1–8 (2002).

65. Anand, P., Elderfield, H. & Conte, M. H. Calibration of Mg/Ca thermometry in planktonic foraminifera from a sediment trap time. *Paleoceanography* **18**(2), 10502002PA000846 (2003).
66. Bemis, B. E., Spero, H. J., Bijma, J. & Lea, D. W. Re-evaluation of the oxygen isotopic composition of planktonic foraminifera: Experimental results and revised paleotemperature equations. *Paleoceanography* **13**(2), 150–160 (1998).
67. Shackleton, N. J. The 100,000-Year Ice-Age Cycle identified and found to lag temperature, carbon dioxide, and orbital eccentricity. *Science* **289**(5486), 1897–1902 (2000).
68. McCabe, G. J., Palecki, M. A. & Betancourt, J. L. Pacific and Atlantic Ocean influences on multidecadal drought frequency in the United States. *Proc. Nat. Acad. Sci.* **101**(12), 4136–4141 (2004).
69. Harris, I., Jones, P. D., Osborn, T. J. & Lister, D. H. Updated high-resolution grids of monthly climatic observations – the CRU TS3.10 dataset. *Int. J. Climatol.* **34**, 623–642 (2014).
70. Rayner, N. A. *et al.* Global analyses of sea surface temperature, sea ice, and night marine air temperature since the nineteenth century. *J. Geophys. Res.* **108**(D14), 4407 (2003).
71. Kothawale, D. R. & Rajeevan, M. Monthly, seasonal and annual rainfall time series for all-India, homogeneous regions and meteorological subdivisions: 1871–2016. Contribution from IITM, Research Report No. RR – 138, ESSO/IITM/STCV/ SR/02(2017)/189.

Acknowledgements

We thank both the anonymous reviewers and Editorial board members for their constructive comments which improved the interpretations. We gratefully acknowledge the financial support given by the European Union under the Marie Curie Grant to PDN and NERC grant to RG. Our sincere thanks to all participants of the cruise MD 161. This is CSIR NIO Contribution 6484.

Author contributions

P.D.N. and R.G. planned the work, M.A.B. computed correlation/regression analyses for the 20th century, C.P. contributed in picking the foraminifera for isotopic and Mg/Ca analyses. Mg/Ca analyses were carried out by D.N., J.F.D. has computed the Kernel cross-correlation analysis. All authors contributed ideas in developing the research, discussed the results and wrote the paper.

Competing interests

The authors declare no competing interests.

Additional information

Supplementary information is available for this paper at <https://doi.org/10.1038/s41598-020-58265-3>.

Correspondence and requests for materials should be addressed to P.D.N.

Reprints and permissions information is available at www.nature.com/reprints.

Publisher's note Springer Nature remains neutral with regard to jurisdictional claims in published maps and institutional affiliations.



Open Access This article is licensed under a Creative Commons Attribution 4.0 International License, which permits use, sharing, adaptation, distribution and reproduction in any medium or format, as long as you give appropriate credit to the original author(s) and the source, provide a link to the Creative Commons license, and indicate if changes were made. The images or other third party material in this article are included in the article's Creative Commons license, unless indicated otherwise in a credit line to the material. If material is not included in the article's Creative Commons license and your intended use is not permitted by statutory regulation or exceeds the permitted use, you will need to obtain permission directly from the copyright holder. To view a copy of this license, visit <http://creativecommons.org/licenses/by/4.0/>.

© The Author(s) 2020